Available online at www.sciencedirect.com
SCIENCE DIRECT
International Journal of Mass Spectrometry 249–250 (2006) 68–76
International Journal of Mass Spectrometry
www.elsevier.com/locate/ijms

Core-level excitation and fragmentation of chlorine dioxide

R. Flesch, J. Plenge, E. Rühl *

Institut für Physikalische Chemie, Universität Würzburg, Am Hubland, 97074 Würzburg, Germany

Received 10 November 2005; received in revised form 22 December 2005; accepted 27 December 2005
Available online 3 February 2006

Abstract

Inner-shell excitation and fragmentation of chlorine dioxide (OClO) in the Cl 2p- and O 1s-excitation regime is reported. The electronic structure of the element-selectively excited radical is studied by X-ray absorption and total cation yields. A comparison of both approaches allows us to estimate the absolute photoionization cross-section and the ionization yield near the Cl 2p- and O 1s-absorption edges. The latter quantity is characteristically enhanced in core-ionization continua. We observe below both core-absorption edges intense core-to-valence-transitions. These are assigned in comparison with related work on core-excited sulfur dioxide. These results give clear evidence that the highest molecular orbital of OClO is half-filled. High-resolution spectra recorded in the Cl 2p-regime show evidence for Rydberg transitions. The extrapolation of the term values of the low-lying Rydberg states allows us to derive the Cl 2p-ionization energy of OClO. Fragmentation of core-excited OClO is reported. Photoelectron–photoion-coincidence (PEPICO) spectra are recorded, indicating that singly and doubly charged fragments are formed. Fission of the doubly and multiply charged OClO leads to singly charged fragments. These are measured by photoion–photoion-coincidence (PIPICO) spectra, where characteristic changes in intensity of the fission channels in the Cl 2p- and O 1s-continuum are observed.

Keywords: Chlorine dioxide; Mass spectrometry; Core-level excitation; Photoionization; Fragmentation

1. Introduction

The electronic structure and related properties including excited state dynamics of chlorine dioxide (OClO) have been the subject of numerous experimental and theoretical studies in the past [1–14]. Most of these works are motivated by the occurrence of chlorine dioxide as a trace gas component in the atmosphere. Especially, the abundance of OClO in the polar atmosphere reflects perturbed chlorine chemistry, which has been discussed with respect to ozone loss via photochemical pathways. These may involve photoisomerization into the labile ClOO [15–19].

Several investigations on OClO were focused on UV photoexcitation and possible competing photodissociation channels of low-lying electronically excited states [1,15,16,18,19]. Properties of higher-excited neutral and singly charged ionic states of OClO have also been investigated [7,10]. The photoabsorption spectrum of OClO in the vacuum ultraviolet (VUV) reveals several series of Rydberg states converging to the respective ionization limits [7,10]. No experimental data on photoabsorption of OClO above 25 eV have been published to the best of our knowledge.

The He(I) photoelectron spectrum of OClO has been recorded earlier [7,9]. It has been the subject of a later reinterpretation, where the Franck–Condon factors were calculated and the allowance for anharmonicity as well as the Duschinsky effect were included [13]. Photoionization and fragmentation of ionic OClO have been reported [7,8]. Photoionization mass spectrometry of OClO has revealed a number of singly charged photofragments after excitation with VUV radiation. Apart from the stable parent cation, $OClO^+$, fragmentation products (O^+, Cl^+, ClO^+, and $O_2{}^+$) are observed [8]. Especially, the occurrence of a weak $O_2{}^+$ signal has been discussed in terms of isomerization of $OClO^+$ into $ClOO^+$ [8]. Yields of the ionic fragments as a function of the photon energy have been recorded, so that appearance energies are established and fragmentation mechanisms are derived [7,8]. Furthermore, results from electron impact ionization [2,14] and related theoretical work [12,13] were reported before. Electron impact single and double ionization of OClO have been investigated more recently using time-of-flight mass spectrometry and ion–ion-coincidence techniques [14]. These coincidence spectra indicate

* Corresponding author.
E-mail address: eruehl@phys-chemie.uni-wuerzburg.de (E. Rühl).

1387-3806/$ – see front matter © 2006 Elsevier B.V. All rights reserved.
doi:10.1016/j.ijms.2005.12.046

that $OClO^{++}$ dissociates to form the cation pairs $O^+ + ClO^+$ and $O^+ + Cl^+$.

We report in this work inner-shell excitation and fragmentation of chlorine dioxide. The energy regime investigated focuses on the inner-shell absorption edges of Cl 2p (200–250 eV) and O 1s (525–560 eV). Photoexcitation in these energy regimes allows us to probe the electronic structure and fragmentation after element-selective excitation. Photoabsorption and total cation yields give specific information on the electronic structure and the unoccupied electronic levels in the core-level excitation regime. The results are assigned in comparison with the well-known stable molecular species sulfur dioxide [20–23]. A comparison of the total cation yield with the photoabsorption cross-section allows us to estimate the total photoionization cross-section and the ionization yield, i.e., the number of cations formed per absorbed photon. The fragmentation products that are formed after inner-shell excitation are identified via coincidence experiments, such as photoelectron–photoion-coincidences (PEPICO) and photoion–photoion-coincidences (PIPICO). These results are compared to earlier electron impact work, where ion–ion-coincidences were reported [14].

2. Experimental

The experiments reported in this work are carried out at the electron storage ring facilities BESSY-I and BESSY-II, where the beamlines HE-TGM-2 [24], SX-700-I [25], and U-49-SGM [26] were used. The photon bandwidth of the X-ray monochromators ($E/\Delta E$) is of the order of 300–600 (HE-TGM-2 at BESSY-I) and $\sim 10^4$ (SX-700-I and U-49-SGM at BESSY-II), respectively. The energy scale is calibrated by using well-known near-edge structure of argon (Ar 2p), molecular chlorine Cl_2 (Cl 2p), and molecular oxygen O_2 (O 1s) [27]. The experiments reported on the Cl 2p-edge are recorded at high resolution using the SX-700-I (BESSY-I) and the U-49-SGM (BESSY-II), whereas those measured at the O 1s-edge are taken with low resolution at the HE-TGM-2 (BESSY-I). Photoabsorption cross-sections are measured by using a gas cell of 30 cm length at a total pressure of typically ~0.5 mbar. The absolute pressure in the absorption cell is measured by a capacitance manometer, similar to Ref. [28]. Sodium salicylate is used as a quantum converter for the detection of monochromatic synchrotron radiation, so that a photomultiplier is used for VUV photon detection [29]. The absolute photoabsorption cross-section of OClO is derived near core-level absorption edges by using the pressure dependence of the photoabsorption signal, yielding a linear behavior in the pressure regime under investigation. We estimate the accuracy of the absolute photoabsorption cross-section to be ~15%, similar to earlier work [28].

Photoelectron–photoion-coincidences (PEPICO) and photoion–photoion-coincidences (PIPICO) are measured similar to earlier work [30,31]. Briefly, a time-of-flight mass spectrometer is operated with an electric field strength of 300 V/cm in the ionization region, where constant extraction voltages are applied. The PEPICO spectra are recorded by using a multi-hit TDC (MIPSYS: FLY TDC [30]), which is operated with a typical time resolution of 4 ns, and PIPICO spectra are measured using a time-to-amplitude converter (TAC) [31], respectively.

The gaseous sample of chlorine dioxide is freshly prepared, according to the standard procedure via the reaction of chlorine with sodium chlorite [32]. The sample is immediately used for the experiments without further purification. The conversion of molecular chlorine into the product becomes incomplete after some time, so that the sample may contain traces of Cl_2. This is avoided by monitoring the purity of the sample during the experiments by photoionization mass spectrometry. As a result, no traces of Cl_2 are found in the spectra.

3. Results and discussion

3.1. Electronic structure

Fig. 1 shows a comparison of the photoabsorption cross-section (Fig. 1(a)) with the total cation yield of OClO (Fig. 1(b)) in the Cl 2p-regime. The Cl 2p-edge is characterized by several narrow and broad features and a characteristic increase in the Cl 2p-continuum ($E > 212$ eV), where also broad continuum features are observed. The assignment of these spectral features, the determination of the absolute cross-sections, and the

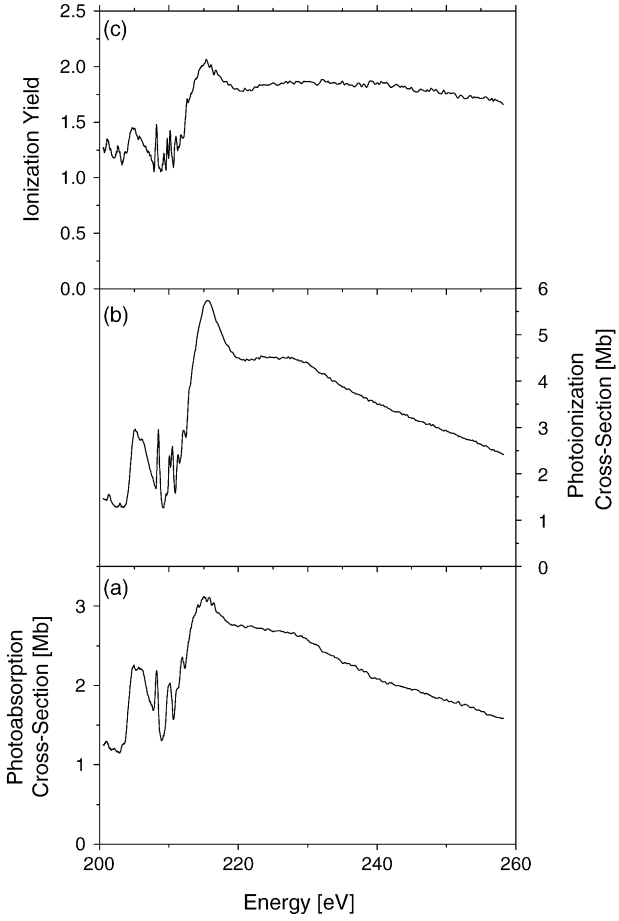

Fig. 1. Comparison of: (a) the photoabsorption cross-section, (b) the photoionization cross-section (derived from the total cation yield), and (c) the ionization yield of chlorine dioxide near the Cl 2p-edge.

determination of the Cl 2p-ionization energies are discussed in greater detail below.

The photoabsorption cross-section of OClO is determined from a photoabsorption experiment, as outlined in the previous section. The results indicate that the discrete features and the continuum intensity have a cross-section of ca. 1–2 Mb, where 1 Mb corresponds to 10^{-22} m^2. These absorption features are superimposed to an intense valence continuum, which has a cross-section of ∼1 Mb. This value as well as the absorption cross-section in the Cl 2p-continuum are in agreement with estimates that take the atomic mass absorption coefficient of chlorine and oxygen into account [33].

The intensity distribution of the total cation yield is in the regime of the near-edge features somewhat enhanced, but similar to the photoabsorption cross-section (see Fig. 1(b)). However, one observes that the cation intensity is significantly enhanced in the Cl 2p-continuum ($E > 212$ eV) compared to the photoabsorption cross-section. The total cation yield shown in Fig. 1(b) is measured on a relative intensity scale. It is subsequently calibrated to an absolute scale by assuming that the photoionization cross-section is similar to the photoabsorption cross-section below the Cl 2p-edge. This implies that the cross-section of neutral states is negligibly small and that the quantum yield of double ionization is ∼20%, corresponding to an ionization yield of ∼1.2. These assumptions appear to be realistic in comparison with earlier work on photoionization of rare gases [34]. We derive from this the photoionization cross-section, corresponding to the absorption cross-section multiplied by the number of charges that are formed per absorbed photon. This yields in the Cl 2p-regime at 215.2 eV a maximum of 5.8 Mb. We note that this approach determines only a lower limit of the photoionization cross-section, since we detect cations and it is implicitly assumed that dissociative processes lead to singly charged fragments. This assumption is not fully fulfilled, as we will show below that about 10% of the cation intensity is due to stable, doubly charged fragments in the Cl 2p-regime. This adds to the error limit of the photoionization cross-section, which is estimated to be of the order of 20%. The photoionization cross-section drops above 215 eV, similar to the photoabsorption cross-section, but it is always higher than the photoabsorption cross-section.

The ionization yield is obtained from the ratio of the photoionization cross-section and the photoabsorption cross-section (see Fig. 1(c)), where only a lower limit of this quantity can be derived. This is on one hand due to the formation of stable dications, on the other hand discrimination effects in cation detection of products that are formed with high kinetic energy from dissociative double ionization are not considered. The ionization yield starts at ∼1.2 in the pre-edge regime (see Fig. 1(c)), implying that more than one cation is formed per absorbed soft X-ray photon and that most dications are not stable and undergo fission, corresponding to the formation of singly charged fragments via charge separation. This assumption is valid, as will be discussed below in the context of fission processes. Furthermore, this value is reasonable, since direct double ionization is of low cross-section (cf. [34]). The substantial cation intensity in the Cl 2p-continuum implies that the ionization yield is significantly enhanced in this spectral regime, where double and multiple

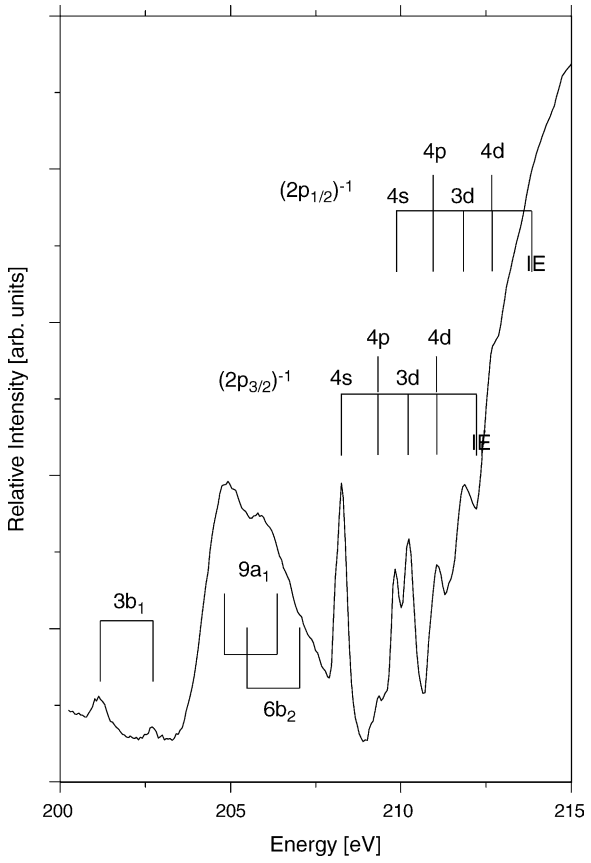

Fig. 2. Total cation yield of OClO with spectral assignments (see text and Table 1 for further details).

ionization become prominent as a result of the preceding LMM-Auger processes. As a result, the ionization yield reaches a value of ∼2 near 215 eV. It drops to 1.8 at higher energy, indicating that still ∼15% of the photoionization processes are due to single ionization. This is reasonable, since the underlying valence continuum has still a considerable strength (∼1 Mb) above the Cl 2p-edge (see Fig. 1(a)). We note that the present results are comparable to earlier work on organometallic species, where a similar increase in ionization yield has been observed in the C 1s-regime [35].

The results also indicate that resonant core-to-valence and core-to-Rydberg states occurring in the Cl 2p-near-edge regime do not contribute significantly to an enhanced ionization yield, so that the ionization yield reaches no larger values than 1.45 ± 0.05 in the pre-edge regime (see Fig. 1(c)). This is because resonant Auger processes do not massively change the ionization yield, which is unlike electronic relaxation via the normal and double Auger processes, dominating the Cl 2p-continuum.

The electronic states occurring near the inner-shell absorption edges are discussed and assigned in the following (cf. Fig. 2). Their assignment is primarily based on previous work on sulfur dioxide (SO_2) [21,36]. This approach is straightforward, since SO_2 has almost the same electronic structure as chlorine dioxide. However, there is one important difference, which concerns the highest occupied molecular orbital (HOMO). In the case of SO_2 the HOMO corresponds to the $8a_1$ orbital, which is dou-

bly occupied, whereas the lowest unoccupied molecular orbital (LUMO) of SO_2 $3b_1$ is empty [21]. This is unlike the electronic structure of OClO, where the extra electron in the HOMO is located in the $3b_1$ orbital, which can be associated with an antibonding π^*-orbital. This singly occupied orbital accounts for the radical character of OClO, with an electronic $\tilde{X}(^2B_1)$ ground state, belonging to the point group C_{2v}, where the bond angle is 117.6° and the Cl–O bond length is 1.47 Å (cf. [16]). The lowest energy transition from the Cl 2p orbital to unoccupied states corresponds to the Cl $2p \rightarrow 3b_1$-transition near 202 eV. The corresponding transition in SO_2 (S $2p \rightarrow 3b_1$) is of weak cross-section, which is a result of the $\Delta l = 1$ selection rule, where it is assumed that the $3b_1$ orbital has predominately p-character. The same is observed for OClO. Consistently, the O $1s \rightarrow 3b_1$-transition in SO_2 and OClO is significantly stronger, as will be outlined below. The $2p \rightarrow 3b_1$-transition is vibrationally resolved in the case of SO_2 [21]. The results on OClO shown in Figs. 1(b) and 2 (total cation yield) indicate that the Cl $2p \rightarrow 3b_1$-transition is split by ~1.6 eV as a result of spin–orbit splitting. In addition, there is no evidence for vibrational fine structure of this transition, which is not a result of the bandwidth of the X-ray monochromator ($E/\Delta E = 10^4$). We assign these continuous bands to the short-lived or dissociative character of the final state. This is unlike SO_2, since in the case of OClO the $3b_1$ orbital is already half-filled, so that the cross-section is expected to be even weaker than in SO_2 and the excitation process brings a second electron into the antibonding final state. This leads to a decrease in bond order. As a result, this excited state is expected to be dissociative or its lifetime is considerably shorter than in SO_2, implying that there will be a significant increase in line width, so that no vibrational fine structure can be observed.

The broad structure occurring near 206 eV is assigned in analogy to SO_2 to two blended transitions, corresponding to the Cl $2p \rightarrow 9a_1$- and Cl $2p \rightarrow 6b_2$-transitions (cf. Fig. 2). These are due to excitations of the 2p-electrons into π^*-orbitals. They are blended in the case of OClO, which is partly due to spin–orbit splitting. A spectral de-convolution indicates that the broad, barely structured band consists of four components that fully explain this band (cf. Fig. 3). At the high-energy portion of this band there is an intense, narrow feature. This is assigned to the lowest Rydberg transition (Cl $2p_{3/2} \rightarrow 4s$, $E = 208.25$ eV, see Figs. 1 and 2). The regime of Rydberg transitions is located near the edge jump, where the density of states increases and the absorption and ionization cross-sections are enhanced. We observe only the lowest members of three different Rydberg series, converging to the $2p_{3/2}$ and $2p_{1/2}$ ionization energies, respectively (see Fig. 2). Their assignments are based on typical term values and constant quantum defects (see Fig. 2 and Table 1). The results compiled in Fig. 2 indicate that the Rydberg series of each fine structure component have the same convergence limit, if the quantum defects that are listed in Table 1 are assumed to be constant. This yields the Cl 2p-ionization energies (IE(Cl 2p)) of OClO 212.23 ± 0.05 eV (IE(Cl $2p_{3/2}$)) and 213.83 ± 0.05 eV (IE(Cl $2p_{1/2}$)), respectively. Note that these core-ionization energies have not been reported to the best of our knowledge. The present approach to determine the Cl 2p-ionization energies in OClO makes use of the lowest Rydberg states. It can only yield an estimate of IE(Cl 2p) in OClO, since higher members of the Rydberg series are not accessible. Alternatively, one can consider to measure X-ray photoelectron spectra (ESCA [37] or zero kinetic energy (ZEKE) photoelectron spectra [38]). Both approaches are expected to yield similar values compared to the present results, where the absolute values of the Cl 2p-ionization energies are estimated to be at most by ±0.3 eV off the values derived in this work. This deviation is small compared to the Cl 2p-ionization energy of molecular chlorine, which is known to be at 207.82 eV (IE(Cl $2p_{3/2}(Cl_2)$))

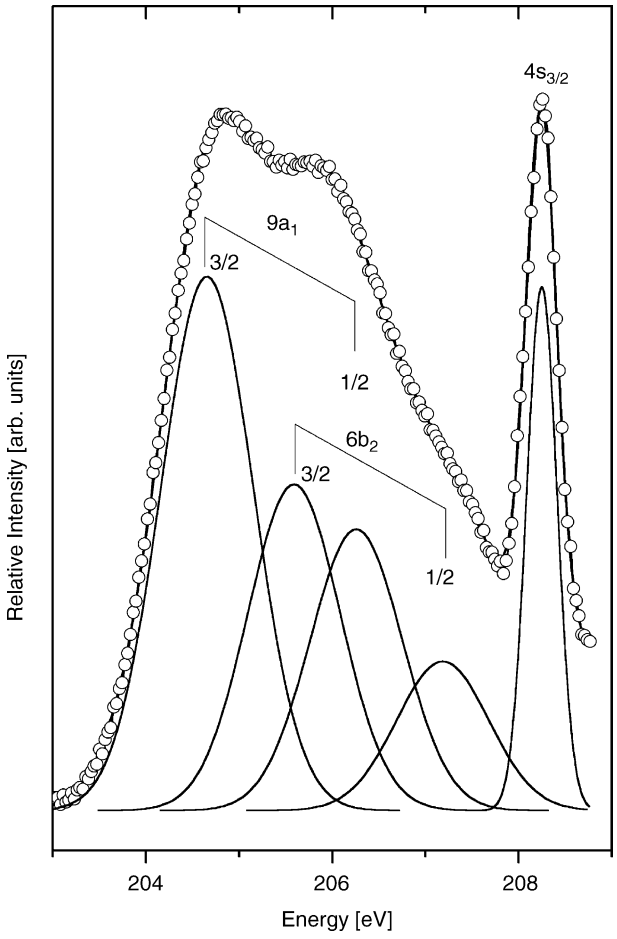

Fig. 3. Total cation yield of OClO with spectral de-convolutions and assignments by using Gaussian line profiles. The hollow circles correspond to the experimental results, the thick line is the sum of all components, thin lines correspond to the Gaussian profiles.

Table 1
Rydberg transitions of OClO near the Cl 2p-edge

Energy (eV)	Assignment	Quantum defect	Term value	Ionization energy (eV)
208.25	$4s_{3/2}$	2.15	3.98	212.23
209.29	$4p_{3/2}$	1.85	2.94	212.23
209.80	$4s_{1/2}$	2.16	4.02	213.82
210.18	$3d_{3/2}$	0.42	2.04	212.22
210.89	$4p_{1/2}$	1.84	2.92	213.81
211.05	$4d_{3/2}$	0.60	1.18	212.23
211.81	$3d_{1/2}$	0.41	2.03	213.84
212.65	$4d_{1/2}$	0.61	1.18	213.83

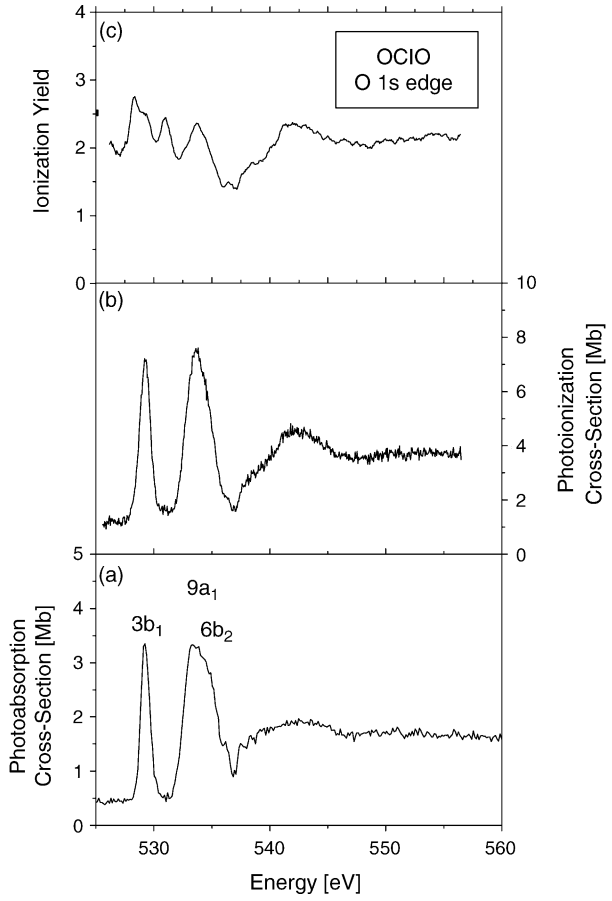

Fig. 4. Comparison of: (a) the photoabsorption cross-section, (b) the photoionization cross-section (derived from the total cation yield), and (c) the ionization yield of chlorine dioxide near the O 1s-edge.

[39]. This implies that molecular chlorine undergoes a significant chemical shift of 4.4 eV, if it is oxidized to OClO.

The Cl 2p-continuum shows an intense feature near 215 eV and a weak one near 230 eV (cf. Fig. 1). These are primarily assigned to shape resonances, which is in analogy to recent work on 2p-excited sulfur dioxide [22]. Moreover, the O^- yield from S 2p-excited SO_2 indicates that there is in the same spectral regime evidence for weak doubly excited states [22]. Such features may be blended with the broad shape resonances and cannot be identified in the case of 2p-excited OClO.

Finally, there is a strong background continuum visible in Fig. 1, which is underneath the Cl 2p-edge. This background has an intensity that reaches ∼25% of the total intensity at 215 eV. It is assigned to photoionization of valence orbital electrons, which still have a significant cross-section in the Cl 2p-regime [33], as outlined above.

The photoabsorption cross-section and the total cation yield of OClO in the O 1s-excitation regime are shown in the energy regime 525–560 eV (cf. Fig. 4). Both spectra are recorded with lower energy resolution ($E/\Delta E \approx 500$) than the results recorded at the Cl 2p-edge (see Figs. 1–3). The Cl 2p- and the valence-continua are weak in the pre-edge regime, accounting for ca. 0.5 Mb of photoabsorption cross-section (see Fig. 4(a)). This is in agreement with Ref. [33] and related work on SO_2 [40]. The photoabsorption cross-section reaches ca. 3 Mb at the maximum of the near-edge features, which is discussed below. It drops in the O 1s-continuum to ∼1.5 Mb. This value is higher than 0.9 Mb, which is expected from the atomic absorption cross-section (cf. [33]). This indicates that broad continuum features increase the photoabsorption cross-section in the 540–560 eV regime. The total cation yield is shown in Fig. 4(b). It is similar in shape compared to the photoabsorption cross-section, i.e., the intensity ratio of the discrete and the continuum features is not significantly changed. This is unlike the results shown in the Cl 2p-regime, where considerably higher intensity is found in the Cl 2p-continuum in the total cation yield than in the photoabsorption cross-section (see Fig. 1). We have estimated the photoionization cross-section of O 1s-excited OClO by using the total cation yield, which is scaled by the photoabsorption cross-section in the pre-edge regime, similar to the Cl 2p-regime. Fig. 1(c) indicates an ionization yield near the Cl 2p-edge of 1.8. This quantity is expected to increase slightly with photon energy, since the valence continuum gets weaker with energy. Similar findings are reported in the literature for rare gases [34]. Therefore, we assume that the ionization yield is ∼2 below the O 1s-edge. This takes into account that there is predominantly dissociative double ionization besides with lower efficiency single and dissociative triple ionization. Especially, the latter process is induced by shake-off events. We use the ionization yield of ∼2 to scale the total cation yield in order to estimate the photoionization cross-section, as shown in Fig. 4(b). Its maximum of ∼8 Mb is reached at the intense discrete feature near 531 eV and it drops in the O 1s-continuum, where ∼4 Mb is found. Note that the derived values also represent a lower limit, since stable dications contribute to ∼15% of the cation yield in this spectral regime. Therefore, we underestimate the photoionization cross-section similar to the discussion given above on the Cl 2p-regime. Finally, the ionization yield is displayed in Fig. 4(c). The results indicate that this quantity is roughly constant in the entire spectral O 1s-regime. Slight modulations are due to the near-edge features, but it needs to be pointed out that the spectra shown in Fig. 4(a) and (b) are recorded with slightly different bandwidth, so that this leads to modulations of the ionization yield, which are not significant. The result, that there is no change in ionization yield below and above the O 1s-edge is rationalized as follows: Excitation of the O 1s-edge does not increase the degree of ionization of OClO, since the Cl 2p-continuum already produces preferably doubly charged OClO. This is not changed in the O 1s-continuum, but different processes gain intensity, especially those that are related to the KLL-Auger decay of core-excited oxygen.

The O 1s-near-edge regime is characterized by two intense bands centered at 529.70 eV and near $E = 533.5$ eV (cf. Fig. 4). The latter feature is significantly broader than the former one. Moreover, its shape is asymmetric, indicating that at least two transitions are blended in this feature. These bands are followed by continuous absorption that contains broad features in the O 1s-continuum, where both the absorption and ionization cross-sections drop with increasing photon energy. A spectral de-convolution of the spectral regime between 527 and 536 eV is performed by using Gaussian fit functions (see Fig. 5). It reveals

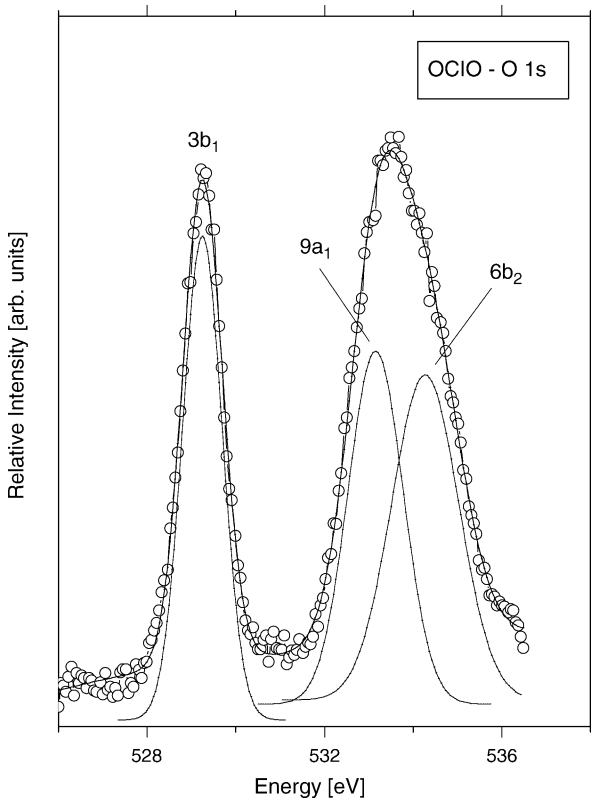

Fig. 5. Total cation yield of OClO with spectral de-convolutions and assignments by using Gaussian line profiles. The hollow circles correspond to the experimental results, the thick line is the sum of all components, thin lines correspond to the Gaussian profiles (cf. Table 2).

that three core-to-valence-transitions occur. This becomes evident for the feature at 529.70 eV, which contains only a single transition. It is assigned to the O 1s → $3b_1(\pi^*)$-transition. This is in agreement with the assignment of the weak, lowest energy near-edge Cl 2p-feature (see above). Such spectral features are well-known to occur in the near-edge regime of numerous unsaturated molecules, where intense bands of π^*-character are observed [27]. This is also similar to the O 1s-absorption of SO_2, where similar characteristics have been found [20,41,42]. There is, however, a distinct difference in the absorption of OClO, where the intensity of the O 1s → $3b_1$-transition is significantly reduced to about half of the intensity compared to the corresponding transition in O 1s-excited SO_2 (cf. [20,42]) This is due to the fact that the $3b_1(\pi^*)$-orbital is half-filled in OClO and it is empty in the case of SO_2, which explains the lower intensity of this band in Fig. 4.

The following broad structure centered near 533.5 eV is de-convoluted into two components, as shown in Fig. 5. We derive from this de-convolution a splitting of 0.92 eV, which is comparable in magnitude to the $9a_1$–$6b_2$-splitting near the Cl 2p-edge (see Table 2 and Fig. 3). It is therefore plausible to assign both components in analogy to the Cl 2p-edge, corresponding to excitations into σ^*-states. Rydberg states are not resolved in Fig. 4. This is essentially a result of the lower energy resolution compared to the findings obtained near the Cl 2p-edge. Finally, we observe a broad continuum resonance near 542.2 eV. It occurs near the O 1s-ionization threshold, which is not exactly known

Table 2
Spectral features of OClO near the O 1s edge

Energy (eV)	Line width (eV)	Assignment
529.70	1.15	O 1s → $3b_1$
532.98	1.53	O 1s → $9a_1$
533.90	1.87	O 1s → $6b_2$

to the best of our knowledge. We assign this broad feature in analogy to the results from the Cl 2p-edge and recent work [22] to a shape resonance.

3.2. Fragmentation

Fragmentation of core-excited chlorine dioxide is investigated by photoelectron–photoion-coincidences (PEPICO) (cf. Fig. 6). Fig. 6(a) shows the intensity distribution if the Cl 2p-continuum is excited at 215.6 eV. It is for all dominant fragments similar to the O 1s-excited molecule (E = 543.1 eV, cf. Fig. 6(b)). Relative intensities and widths of the coincidence signals are listed in Table 3. The parent cation $OClO^+$ is observed with weak intensity in both spectra. This is unlike valence continuum excitation, where this cation is the dominant cation in photoionization mass spectra [8], indicating that there is effi-

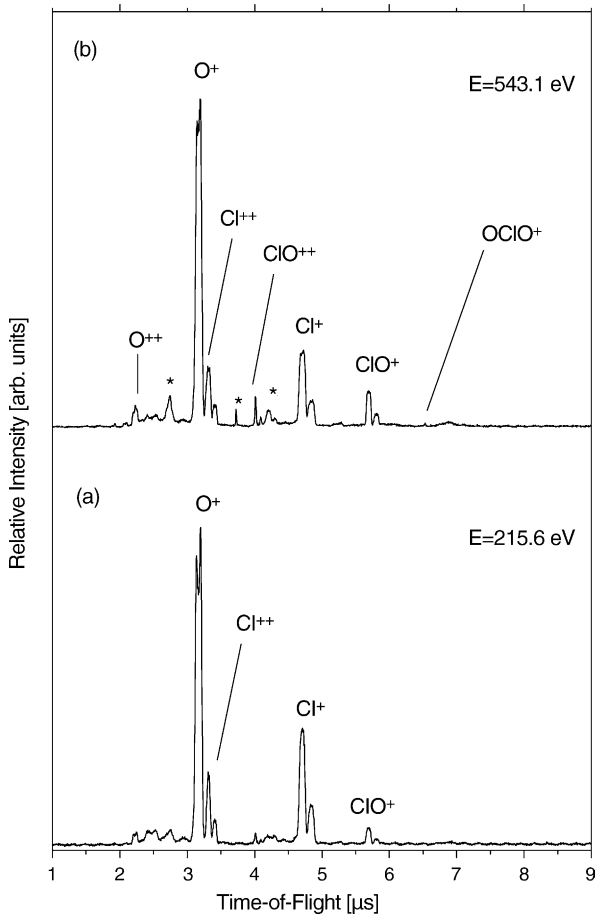

Fig. 6. Photoelectron–photoion-coincidence spectra of OClO recorded at: (a) 215.6 eV and (b) 543.1 eV (see Table 3 for details). Mass signals from traces of air and residual gas are marked by asterisks.

Table 3
Intensities and signal widths of cations produced by photoionization of OClO at 543.1 eV photon energy, as observed by PEPICO spectra (cf. Fig. 6(b))

Cation	Relative intensity (arb. units)	Peak width (ns)
O^+	1146	220
Cl^{++}	206	80
ClO^{++}	33	24
Cl+	358	108
ClO^+	117	76
$OClO^+$	3	28

cient fragmentation in core-ionization continua. Other singly charged fragments that are observed are ClO^+, Cl^+, and O^+. These mass signals are significantly broadened compared to the parent cation $OClO^+$ and the fragment dication ClO^{++}. This is primarily the result of dissociative double ionization of OClO, which is expected to be dominant in the core-ionization continua, where Auger relaxation dominates. This leads to doubly or multiply charged molecules which are stabilized via fission, i.e., the formation of singly charged correlated fragments. Such fragments are detected by multicoincidence experiments. Furthermore, this fragmentation mechanism explains the enhanced photoionization cross-section and ionization yield (see above). As a result of efficient fission, the molecular dication is not observed in Fig. 6. Furthermore, the singly charged fragments are formed via fission. This is accompanied by a substantial kinetic energy release and becomes evident from the increased widths of the mass signals. The most intense cation signal is O^+, whereas the mass lines of the other fragments Cl^+ and ClO^+ are considerably weaker.

Electron impact ionization of OClO was investigated before [14]. There, one observes the singly charged fragments O^+, $O_2{}^+$, Cl^+, and ClO^+ in the electron energy range between 30 and 450 eV [14]. Note that these electron impact mass spectra are dominated by a strong parent signal $OClO^+$ [14], indicating that predominantly the valence shell is excited. The weak formation of $O_2{}^+$ has also been observed before upon excitation by VUV radiation [8]. This cation is evidently exclusively formed via single ionization. Consistently it is not observed in Fig. 6, where double ionization is dominant.

Besides singly charged fragments we also observe doubly charged ones, i.e., Cl^{++} and ClO^{++} (cf. Table 3). The most intense doubly charged fragment is Cl^{++}. The width of this dicationic mass signal is significantly larger than that of the singly charged parent, indicating that Cl^{++} is evidently formed via fission, starting most likely from the triply charged parent. This trication can be formed in the O 1s-continuum via double Auger decay processes. The other observed doubly charged fragment is ClO^{++}. The width of this signal is comparable to that of $OClO^+$. We speculate that this fragment is a result of a process that starts from the dication, where a neutral oxygen atom is formed.

Earlier electron impact work also showed no evidence for a stable parent dication ($OClO^{++}$) [14]. The absence of $OClO^{++}$ has been rationalized by assuming that no bound regions of the dication potential are accessible via a vertical transition from the equilibrium geometry of the neutral $\tilde{X}(^2B_1)$ ground state

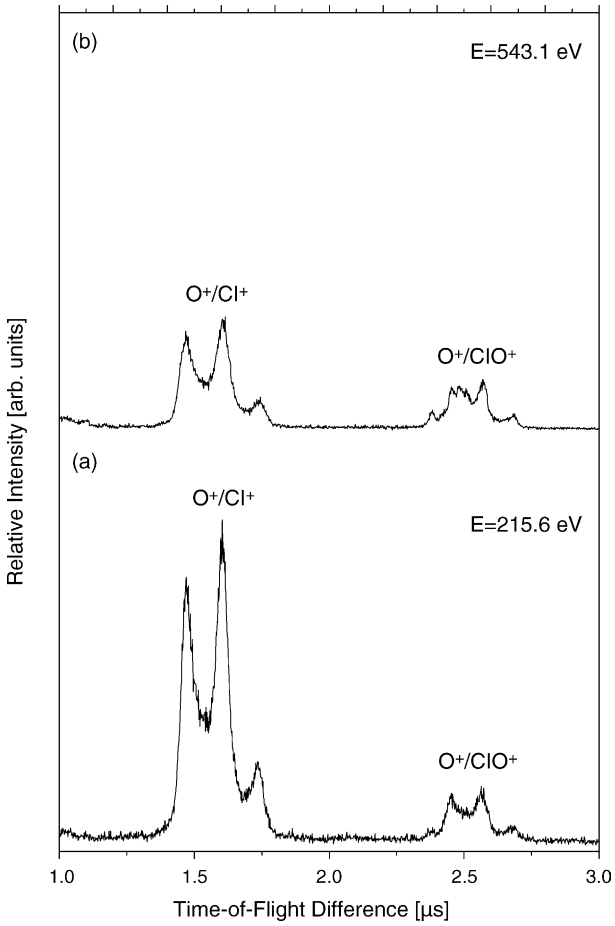

Fig. 7. Photoion–photoion-coincidence spectra of OClO recorded at: (a) 215.6 eV and (b) 543.1 eV.

[14]. Fission mechanisms of doubly charged molecules, leading to the singly charged fragments, are suitably investigated by PEPIPICO spectroscopy [43–46]. Recent work has concentrated on SO_2 [23,45,46] besides a related electron impact study, which includes ion–ion-coincidences [14]. We report in this work results from photoion–photoion-coincidence (PIPICO) spectroscopy (see Fig. 7). This figure shows a comparison of two photoion–photoion-coincidence (PIPICO) spectra recorded at two different photon energies, i.e., at 215.6 eV (Cl 2p-continuum) and 543.1 eV (O 1s-continuum). We focus on the regime between 1 and 3 μs time-of-flight difference and do not discuss the regime of small time-of-flight differences ($\Delta t \approx 0$), since there one finds a broad feature that can have contributions from several channels, such as O^+/O^+, Cl^{++}/O^+, as well as false coincidences. Both PIPCO spectra show the same major signals corresponding to the O^+/Cl^+-coincidence at ∼1.6 μs time-of-flight difference and the O^+/ClO^+-coincidence signal occurring at ∼2.5 μs time-of-flight difference. These coincidence signals have been observed before. The present results are comparable in widths to earlier electron impact work [14], indicating that the kinetic energy release (KER) is comparable to that reported before [14]. Evidently, this quantity is independent on the excitation energy. We do not discuss this point further, but note that evidently the molecular geometry and the charge separation

distance, that can be deduced from the KER according to Coulomb's law, is similar over a wide energy range. However, this is not true for the relative intensities of both coincidence signals. The results reported in Ref. [14] clearly indicate that the O^+/ClO^+-channel is more intense than the other one. This is clearly different from the results shown in Fig. 7. In the O 1s-continuum one finds that the O^+/Cl^+-channel is about twice as intense as the O^+/ClO^+-channel. This situation changes, when the excitation energy is tuned into the Cl 2p-continuum, where this ratio increases to ∼6. This implies that atomization via fission of the doubly charged molecule is dominant upon Cl 2p-excitation. This is remarkable since the Cl 2p-excitation energy is lower than the O 1s-excitation energy. This indicates that atomization of OClO, leading to fission into atomic cations, is not as efficiently induced by high-photon energies, rather than by site-selective excitation and relaxation routes. Chlorine is bound as the central atom in OClO, so that excitation of this central site leads efficiently to the formation of charged atoms via fission. In contrast, the oxygen sites are located at both ends of the molecule, so that excitation of these sites leads with a lower yield to the O^+/Cl^+-cation pair. Site- and element-selective excitation and fragmentation has been discussed for other triatomic, such as N_2O [47], as well as polyatomic molecules before [48]. This earlier work on N_2O revealed, similar to the present results, that excitation of the central atom leads to more massive fragmentation than for the terminal sites. This behavior was ascribed to selective Auger processes, which lead to different cation states. These decay subsequently into the correlated fragments via fission [47]. It is assumed that similar processes occur in OClO.

4. Conclusions

Photoabsorption and photoionization mass spectrometry experiments on core-excited chlorine dioxide (OClO) provide specific information on the electronic structure in the regime of element-selective excitation. We observe intense core-to-valence-transitions that are assigned in comparison with previous results on sulfur dioxide. A comparison between the O 1s-excitation spectra reveals that the absorption and photoionization cross-section of the O $1s \rightarrow 3b_1$-transition is characteristically decreased in OClO, which is a result of the half-filled HOMO (π^*-orbital). In contrast, this molecular orbital is empty in the case of SO_2. Several low-lying members of Rydberg series are identified in the Cl 2p-regime. These are used to estimate the Cl 2p-ionization energies.

Distinct differences between the photoabsorption cross-section and the total cation yield are observed in the Cl 2p-regime, whereas both types of spectra are similar to each other in the O 1s- regime. Total cation yields are used to estimate the lower limit of the photoionization cross-section. A comparison with results from electron ion coincidence experiments yields that the derived values of the photoionization cross-section are slightly underestimated by ∼10–15%. This is essentially due to stable dication formation and discrimination effects of high kinetic energy cation detection. The ratio between the photoionization cross-section and the photoabsorption cross-sections provides the ionization yield, i.e., the number of cations that are produced per absorbed photon. This quantity increases almost to 2 above the Cl 2p-ionization threshold as a result of LMM-Auger processes. The results in the O 1s-regime show that double and multiple ionization dominate below and above this absorption edge, but the ionization yield is not different below and above the O 1s-edge. Finally, photoion–photoion-coincidence spectra show evidence for fission channels that follow double and multiple ionization. A distinct enhancement of the O^+/Cl^+ cation pair relative to that containing O^+/ClO^+ is observed in the Cl 2p-excitation regime. This indicates that this atomic fragment pair is preferably formed upon fission when the central atom is excited.

Acknowledgments

Financial support by the Deutsche Bundesstiftung Umwelt, Deutsche Forschungsgemeinschaft, and Fonds der Chemischen Industrie are gratefully acknowledged.

References

[1] R.P. Wayne, G. Poulet, P. Biggs, J.P. Burrows, R.A. Cox, P.J. Crutzen, G.D. Hayman, M.E. Jenkin, G. Le Bras, G.K. Moortgat, U. Platt, R.N. Schindler, Atmos. Environ. 29 (1995) 2677.
[2] I.P. Fisher, J. Chem. Soc. Faraday Trans. 63 (1967) 684.
[3] C.M. Humphries, A.D. Walsh, P.A. Warsop, Discuss. Faraday Soc. Soc. 35 (1963) 137.
[4] N. Basco, R.D. Morse, Proc. Roy. Soc. A 336 (1974) 495.
[5] E.C. Richard, V. Vaida, J. Chem. Phys. 94 (1991) 153;
E.C. Richard, V. Vaida, J. Chem. Phys. 94 (1991) 163.
[6] E. Rühl, A. Jefferson, V. Vaida, J. Phys. Chem. 94 (1990) 2990.
[7] R. Flesch, E. Rühl, K. Hottmann, H. Baumgärtel, J. Phys. Chem. 97 (1993) 837.
[8] U. Rockland, H. Baumgärtel, E. Rühl, O. Lösking, H.S.P. Müller, H. Willner, Ber. Bunsenges. Phys. Chem. 99 (1995) 969.
[9] A.B. Cornford, D.C. Frost, F.G. Herring, C.A. McDowell, Chem. Phys. Lett. 10 (1971) 345;
A.B. Cornford, D.C. Frost, F.G. Herring, C.A. McDowell, Discuss. Faraday Soc. 54 (1972) 56.
[10] S. Hubinger, J.B. Nee, Chem. Phys. 181 (1994) 247.
[11] E. Bishenden, D.J. Donaldson, J. Chem. Phys. 99 (1993) 3129;
E. Bishenden, D.J. Donaldson, J. Chem. Phys. 101 (1994) 9565.
[12] K.A. Peterson, H.-J. Werner, J. Chem Phys. 99 (1993) 302.
[13] D.K.W. Mok, E.P.F. Lee, F.-T. Chau, D. Wang, J.M. Dyke, J. Chem. Phys. 113 (2000) 5791.
[14] C.S.S. O'Connor, N. Tafadar, S.D. Price, J. Chem. Soc. Faraday Trans. 94 (1998) 1797.
[15] M. Weber, K.U. Eichmann, F. Wittrock, K. Bramstedt, L. Hild, A. Richter, J.P. Burrows, R. Müller, Quart. J. Roy. Met. Soc. 128 (2002) 1293.
[16] V. Vaida, S. Solomon, E.C. Richard, E. Rühl, A. Jefferson, Nature 342 (1989) 405.
[17] T. Wagner, C. Leue, K. Pfeilsticker, U. Platt, J. Geophys. Res. 106 (2001) 4971.
[18] W.G. Lawrence, K.C. Clemtishaw, V.A. Apkarian, J. Geophys. Res. 95 (1990) 18591.
[19] K.A. Peterson, H.J. Werner, J. Chem. Phys. 96 (1992) 8948;
K.A. Peterson, H.J. Werner, J. Chem. Phys. 105 (1996) 9823.
[20] K.H. Sze, C.E. Brion, X.M. Tong, J.M. Li, Chem. Phys. 115 (1987) 433.
[21] E. Gedat, R. Püttner, M. Domke, G. Kaindl, J. Chem. Phys. 109 (1998) 4471.
[22] W.C. Stolte, R. Guillemin, A. Wolska, R. Feng, I.C. Tran, D.W. Lindle, J. Electron Spectrosc. Relat. Phenom. 144–147 (2005) 157.

[23] R. Feng, R.G. Cavell, A.P. Hitchcock, J. Electron Spectrosc. Relat. Phenom. 144–147 (2005) 231.
[24] S. Bernstorff, W. Braun, M. Mast, W. Peatman, T. Schroeter, Rev. Rev. Sci. Instr. 60 (1989) 2097.
[25] H. Petersen, H. Baumgärtel, Nucl. Instrum. Meth. 172 (1980) 191; H. Petersen, C. Jung, C. Hellwig, W.B. Peatman, W. Gudat, Rev. Sci. Instrum. 66 (1995) 1.
[26] F. Senf, F. Eggenstein, U. Flechsig, R. Follath, S. Hartlaub, H. Lammert, T. Noll, J.S. Schmidt, G. Reichardt, O. Schwarzkopf, M. Weiss, T. Zeschke, W. Gudat, Nucl. Instrum. Meth. A 467 (2001) 474.
[27] A.P. Hitchcock, D.C. Mancini, J. El. Spectrosc. Relat. Phenom. 67 (1994) 1.
[28] E. Rühl, H.W. Jochims, H. Baumgärtel, Can. J. Chem. 63 (1985) 1949.
[29] J.A.R. Samson, Techniques of Vacuum Ultraviolet Spectroscopy, Wiley, New York, 1967.
[30] E. Rühl, Int. J. Mass Spectrom. 229 (2003) 117, and references therein.
[31] E. Rühl, C. Schmale, H.W. Jochims, E. Biller, M. Simon, H. Baumgärtel, J. Chem. Phys. 95 (1991) 6544.
[32] R.I. Derby, W.S. Hutchinson, Inorg. Synth. 4 (1953) 152.
[33] M. Thomas, Optical Grapher Program, Center of X-Ray Optics, U.C. Berkeley, 1991.
[34] N. Saito, I.H. Suzuki, Int. J. Mass Spectrom. 115 (1992) 157.
[35] E. Rühl, C. Heinzel, H. Baumgärtel, A.P. Hitchcock, Chem. Phys. 169 (1993) 243.
[36] S. Rothenberg, H.F. Schaefer III, J. Chem. Phys. 53 (1970) 3014.
[37] K. Siegbahn, C. Nordling, G. Johanson, J. Hedman, P.F. Heden, K. Hamrin, U. Gelius, T. Bergmark, L.O. Werme, R. Manne, Y. Baer, ESCA Applied to Free Molecules, North Holland, 1969.
[38] A. Knop, H.W. Jochims, A.L.D. Kilcoyne, A.P. Hitchcock, E. Rühl, Chem. Phys. Lett. 223 (1994) 553.
[39] W.L. Jolly, K.D. Bomben, C.J. Eyerman, At. Data Nucl. Data Tab. 31 (1984) 433.
[40] A. Jürgensen, R.G. Cavell, Chem. Phys. 257 (2000) 123.
[41] V.N. Akhimov, A.S. Vinogradov, T.M. Zimkina, Opt. Spectrosc. 53 (1983) 548.
[42] T. Gejo, Y. Takata, T. Hatsui, M. Nagasono, H. Oji, N. Kosugi, E. Shigemasa, Chem. Phys. 289 (2003) 15.
[43] J.H.D. Eland, Mol. Phys. 61 (1987) 725.
[44] E. Rühl, S.D. Price, S. Leach, J.H.D. Eland, Int. J. Mass Spectrom. Ion Proc. 97 (1990) 175.
[45] M. Lavollée, V. Brems, J. Chem. Phys. 110 (1999) 918.
[46] B.O. Fisher, M.K. Thomas, P.A. Hatherly, K. Codling, M. Stankiewicz, A. Karawajczyk, M. Roper, J. Phys. B 32 (1999) 4437.
[47] J. Murakami, M.C. Nelson, S.L. Anderson, D.M. Hanson, J. Chem. Phys. 85 (1986) 5755.
[48] C. Miron, M. Simon, N. Leclercq, D.L. Hansen, P. Morin, Phys. Rev. Lett. 81 (1998) 4104.